Phenomenological modeling of durotaxis

Guangyuan Yu, Jingchen Feng, Haoran Man, and Herbert Levine

Phys. Rev. E **96**, 010402 — Published 17 July 2017

DOI: 10.1103/PhysRevE.96.010402

Phenomenological Modeling of Durotaxis

Guangyuan Yu[1,2], Jingchen Feng[2], Haoran Man[1],Herbert Levine[2,3]
[1] *Physics and Astronomy Department, Rice University, Houston, USA*
[2] *Center for Theoretical Biological Physics, Rice University, Houston, USA*
[3] *Bioengineering Department, Rice University, Houston, USA*
(Dated: June 28, 2017)

Cells exhibit qualitatively different behaviors on substrates with different rigidities. The fact that cells are more polarized on the stiffer substrate motivates us to construct a two-dimensional cell with the distribution of focal adhesions dependent on substrate rigidities. This distribution affects the forces exerted by the cell and thereby determines its motion. Our model reproduces the experimental observation that the persistence time is higher on the stiffer substrate. This stiffness dependent persistence will lead to durotaxis, the preference in moving towards stiffer substrates. This propensity is characterized by the durotaxis index first defined in experiments. We derive and validate a 2D corresponding Fokker-Planck equation associated with our model. Our approach highlights the possible role of the focal adhesion arrangement in durotaxis.

Cells are capable of sensing and responding to the mechanical properties of their external environment. For example, cytoskeletal stiffness [1], cellular differentiation [2–5] and cell morphology and motility [6–9] are all strongly influenced by ECM stiffness. In particular, it has been shown experimentally that cells prefer crawling towards the stiffer parts on substrates with spatially varying rigidity, a property which is referred to as durotaxis. Durotaxis is a universal property of motile cells, despite the diverse shapes and structures among different cell types. It has been proposed that durotaxis is critical for fine-tuning cell path-finding and wound healing [10, 11]. Also, there is increasing evidence showing that durotaxis is involved in cancer metastasis, since tumors are usually stiffer than the surrounding materials [12, 13].

A standard approach to modeling cell motility is to assume that cells execute a persistent random walk [14–16]; sometimes Lévy walks are used instead [17, 18]. Recently, Novikova and colleagues applied persistent random walk ideas to understand durotaxis by relating persistence to substrate stiffness [19]. Their approach did show how this assumption could lead to durotaxis, but did not propose any direct mechanical reason for this correspondence; also they did not fully analyze their model in the relevant case of a two-dimensional spatial domain. In this study, we propose a simple intracellular mechanism that naturally leads to stiffness dependent persistence which, in agreement with the above findings, results in durotaxis. Our approach combines direct simulations with the derivation of a quantitatively accurate 2D Fokker-Planck equation, for which the numerical solution matches well with simulation data.

Our basic hypothesis is built on the fact that cells are observed to be more polarized when they move on stiffer materials. Cells have sophisticated mechanisms to sense stiffness, involving various cellular components and subsystems including the plasma membrane [20, 21], actin filaments [22, 23], actomyosin-based contractility, integrin-based focal adhesions [24, 25], etc. Once cells sense a stiffer substrate, they take on a more elongated shape [26, 27] as a response. Now, cells move by protrusions which occur with the help of focal adhesions which allow force transmission to the substrate. We will assume that the change in shape to being more polarized implies that focal adhesions (FA) are formed within a narrower wedge on the cell front. In other words, we assume that the FA distribution is correlated with cell polarization; the exact biophysical process which creates this correlation is not addressed here. It is also possible that the total number of FAs present at some fixed time increases on stiffer substrates, as FA are observed to be more stable on stiffer substrates [6]. In our model, both the distribution and the total number of FA directly control the variance of deflection angles in cell motion over a short time interval. We also consider the possibility that cell speed may also depend on stiffness.These mechanisms will create the necessary relationship between stiffness and persistence.

In experiments, the locations of cells moving on a 2D surface are typically recorded at fixed time intervals. Accordingly, we model the cell as a rigid object moving with velocity v and rotating its motion direction Φ (its polarization) by an angle $\Delta\Phi$ at fixed time intervals $\Delta t = t_{i+1} - t_i$ which we take to be our unit of time. To determine $\Delta\Phi$, we assume there are a number N_f of focal adhesions which are positioned at distances r_i from the cell center and angles θ_i relative to the current direction of motion; these are chosen randomly from uniform distributions with ranges (r_{min}, r_{max}), $(-\theta_{max}, \theta_{max})$ respectively. We assume in line with the previous arguments that θ_{max} is determined by local substrate stiffness k as $\theta_{max} = A/k$, where A is a constant factor. The basic picture of our cell is given in Fig. 1, Our calculations will assume that N_f remains constant. The driving force from each focal adhesion is assumed to have a constant magnitude and to point in the current moving direction. The net driving force is canceled by the friction acting on the cell, thereby determining the velocity. It is worth noting that in reality, FA's are located both at the front and the back of the cell. The forces applied by back FAs, which typically operate in a "slipping" rather than "gripping mode" [28] are replaced with friction.

At each time step, the dynamical formation and dis-

ruption of FAs cause a possible imbalance in the driving torque. With fast relaxation, the cell will rotate by an angle $\Delta\Phi$ at each time step to satisfy zero net torque:

$$\sum_{i=1}^{N_f} r_i \sin(\theta_i - \Delta\Phi) = 0 \tag{1}$$

whose solution is:

$$\tan\Delta\Phi = \frac{\sum_{i=1}^{N_f} r_i \sin(\theta_i)}{\sum_{i=1}^{N_f} r_i \cos(\theta_i)} \tag{2}$$

For the purpose of illustration, we typically set $r_i = 1$ for all i and $N_f = 12$ in our model.

Clearly the variance of the induced distribution for $\Delta\Phi$ determines the persistence of the motion. Here we use a Monte Carlo sampling method to evaluate this variance. We use 10^6 sampling steps and have checked that this gives us an accurate evaluation for the range of parameters we have investigated. For the case of fixed radii, we obtain

$$\int\cdots\int_{-\theta_{max}}^{\theta_{max}} \left(\prod_{i=1}^{N_f} \frac{d\theta_i}{2\theta_{max}}\right) \arctan^2\left(\frac{\sum_{i=1}^{N_f}\sin(\theta_i)}{\sum_{i=1}^{N_f}\cos(\theta_i)}\right)$$

One can also compute the variance for the more general situation with a distribution for the radii as well. Typical results of this calculation are shown in Fig 2a. For use later on, we have fitted the data for the case $N_f = 12$ with fixed radii to a simple function of k.

$$\sigma(k) = \frac{1}{\alpha k + \beta} \tag{3}$$

As expected, increasing N_f or decreasing θ_{max} reduces the variance, whether directly or via more averaging. Thus, rigidity-dependent changes in the focal adhesion dynamics can indeed be used to model the mechanism underpinning the persistence-stiffness correlation.

Since focal adhesions are dynamically formed and destroyed, in our model at each time step the locations of all focal adhesions θ_i are reselected with no correlation to their previous value, hence $< \Delta\Phi(t_i)\Delta\Phi(t_{i+1}) >= 0$. Thus on a uniform substrate, approximating the distribution of $\Delta\Phi$ to be Gaussian with the calculated width reduces our model to a version of the worm-like chain, where the mean squared displacement is:

$$\langle x^2\rangle = v^2\tau_p^2\left(\frac{t}{\tau_p} + e^{-\frac{t}{\tau_p}} - 1\right) \tag{4}$$

Here the persistence time is defined as $\tau_p = -\frac{\Delta t}{\ln\langle\cos\Delta\Phi\rangle}$. Since $\langle\cos\Delta\Phi\rangle = e^{-\frac{\sigma^2\Delta t}{2}}$, where $\sigma^2\Delta t = var(\Delta\Phi)$, $\tau_p = \frac{2}{\sigma^2}$. In terms of real numbers for example from Ref [18], we can set $v = 0.5$ μm (per δt), $\delta t = 0.01h$. We the obtain $\sigma^2\delta t \sim 0.05^2$ on stiff substrates and $\sim 0.3^2$ on soft substrates. In this way, we find $\tau_p = 2/\sigma^2 \sim 0.2h$ on soft substrates and $\sim 8h$ on stiff substrates in our simulations.

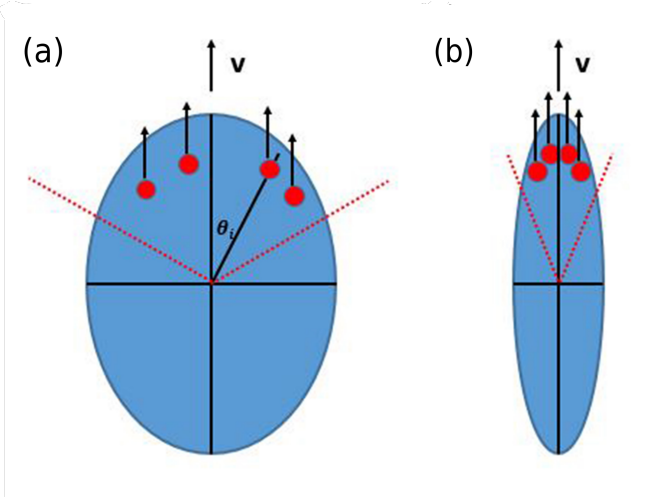

FIG. 1: *A sketch of our model.* Red dots represent focal adhesions. In our simulation, focal adhesions are randomly generated within an angular range bounded by red lines in the figure at each step. (a) For cells on a soft substrate, the distribution of FAs is relatively wide (b) Conversely, for cells on a hard substrate, the distribution of FAs is relatively narrow.

Initially, we assume that the cell speed v is stiffness-independent and we simulate cell trajectories on uniform substrates with different stiffness and verify the previous results for σ^2 (see Fig 2b). In Fig. 2c and 2d, we show trajectories of cells simulated on both uniform soft and hard substrates. Consistent with the experimental observation [29], cells crawl more efficiently on stiffer substrates.

Next, we study the effect of stiffness gradients on cell motility. We impose a constant stiffness gradient in the central region with constant low stiffness k_{left} on the left side and high stiffness k_{right} on the right side. We fix both k_{left} and k_{right} and vary the width of the central region.

$$k(x) = \begin{cases} k_{left} = 1 & -1000 < x < -L \\ k_{left} + \frac{(k_{right}-k_{left})}{2L}(X+L) & -L \le X \le L \\ k_{right} = 5 & L < x < 1000 \end{cases} \tag{5}$$

Initially all our cells are placed at the origin and given a random initial direction. For small width, at a time when half of the cells go into the stiff region on the right, the other half are still hovering within the central gradient region (Fig. 3a). As the width increases, fewer and fewer cells enter the soft region on the left (Fig. 3b and c). This is caused by the fact that larger width allows more moving steps inside the gradient region and cells have more time to adapt to the direction of stiffness gradient. We further characterize these results by the durotactic index (DI) ([30]). We calculate DI defined below every

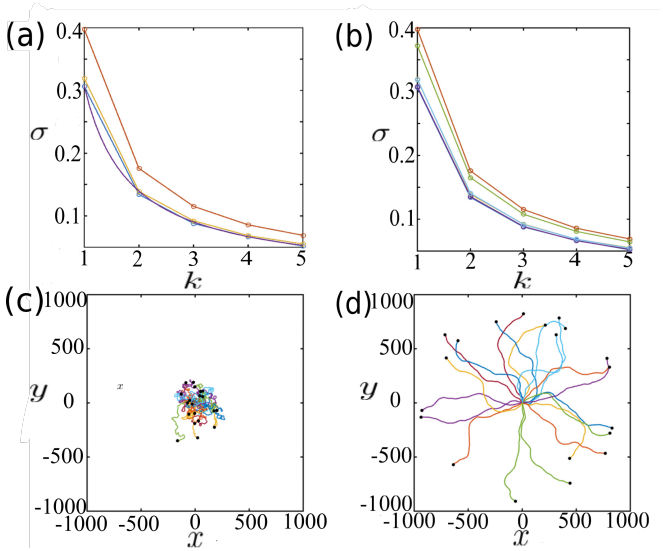

FIG. 2: *Simulation result of uniform substrates and the variance of deflected angles.* (a) The variance of deflected angles calculated by Monte Carlo sampling. σ^2 vs stiffness k. $N = 8, r_i = 1(red)$, $N = 12, r_i = 1(blue)$, $N = 12, r_i \in (0.5, 1.5)$ (yellow) for all i and the fitted function $\sigma(k)$ with $\alpha = 3.9$ and $\beta = -0.645$(Eq 3)(purple). (b) Comparison between Monte Carlo sampling and direct simulation. For $N = 12, r = 1(red)$, two lines overlap together as the purple line. For $N = 12, r_i \in (0.5, 1.5)$, two lines overlap together as the blue line.$N = 8, r_i = 1(green)(directsimulation)$,$N = 8, r_i = 1(red)(MonteCarlo)$. For (c) and (d), we simulate 1000 time steps with $v = 1(arb.units)$ Initial position of 20 cells are (0,0) and the initial moving direction is randomly selected. The black dots are the final positions of each cell. (c) On a soft substrate, k=1 and $\theta_i \in (-0.5\pi, 0.5\pi)$ for all i. (d) On a stiff substrate with k=5, the angle range is $\theta_i \in (-0.1\pi, 0.1\pi)$, for all i.

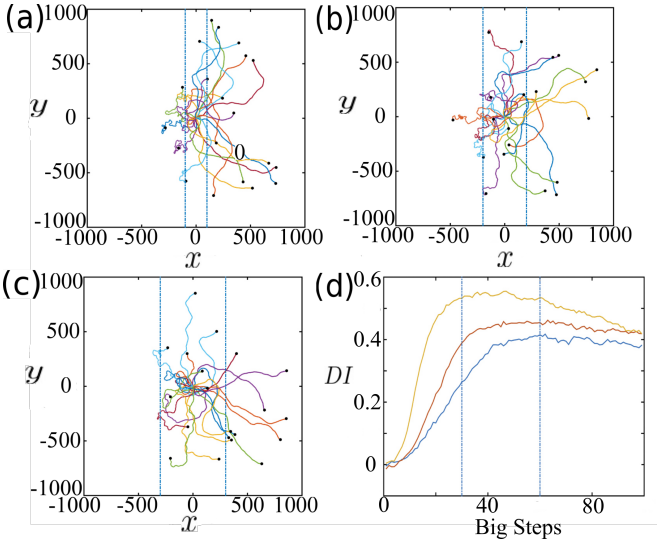

FIG. 3: *Direct simulation on gradient matrix and DI.* (a)-(c) Soft substrate k=1 in the left region and hard substrate k=5 in the right region. The central region has a constant gradient stiffness and varying width L = (a) 100, (b) 200 and (c) 300 (arb. units). (d) Durotaxis Indices at several values of L; the index decreases as L is increased. Every 10 steps is counted as a "big step"

ten time steps in our simulation:

$$Durotaxis\ Index(t_i) = \frac{N_{right} - N_{left}}{N_{right} + N_{left}} \tag{6}$$

where N_{right} and N_{left} are the number of cells have positive and negative net displacement in x-direction respectively. This index ranges from $[-1, 1]$. Larger Durotaxis Indices indicate more cells are moving towards the ascending gradient direction.

We find that the curve can be divided into three sections (Fig. 3d). In the first section, nearly all cells are still in the gradient region. The index increases rapidly, which suggests that cells start being guided by the stiffness gradient. Consistent with experiment observation [27], the magnitude of DI is highly correlated with the magnitude of the gradient. In the second section, part of the cells are in the gradient region while the other have entered the uniform stiffness region. In the last section, the index starts decreasing because all cells move into the uniform rigid region and begin to execute random walks. The DI curve in the first section elucidates the role of gradient stiffness on cell motility.

To facilitate understanding of our simulation data, we now develop a Fokker-Plank equation for the probability distribution $P(x, y, \Phi; t)$ governing a population of particles in our model. We will be specifically interested in cases with a stiffness gradient, which we choose to lie along the x direction. We focus on the variation with x and Φ and introduce $p = \int dy P$ as a two-dimensional density. For any single cell, the next position $x(t + dt)$ depends on the current position and angle via $x(t) + v\cos(\Phi(t))dt$. We can therefore represent a single step in our stochastic process via

$$p(x, \Phi; t + dt) = \int_0^{2\pi} p(x - v\cos(\Phi_0)dt, \Phi_0; t) \\ f(x - v\cos(\Phi_0)dt, \Phi_0 - \Phi)d\Phi_0 \tag{7}$$

where we will use the aforementioned Gaussian approximation

$$f(x, \Phi_0 - \Phi) = a(x)e^{-\frac{(\Phi_0 - \Phi)^2}{2\sigma(x)^2 dt}} \tag{8}$$

Here $a(x) = \sqrt{\frac{1}{2\pi\sigma(x)^2 \mathrm{dt}}}$ is the normalization coefficient as long as the width is significantly smaller than 2π. Note that now the variance depends on x through an x dependence in the stiffness k.

In standard manner we can assume small dt and expand p around the current values of its arguments. After some simplification, we obtain

$$\frac{\partial p}{\partial t} = -\frac{\partial p}{\partial x} v\cos\Phi + \frac{\sigma(x)^2}{2}\frac{\partial^2 p}{\partial \Phi^2} + v\sin\Phi\frac{\partial}{\partial x}[\sigma(x)^2 dt\frac{\partial p}{\partial \Phi}]$$

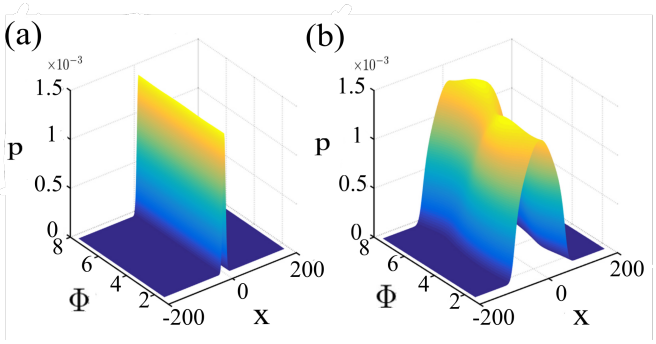

FIG. 4: *PDE solution.* (a) Initial probability density function $p(x, \Phi; t = 0)$ (b) Probability density function $p(x, \Phi; t = 94)$ on a uniform substrate. Note that in this and the subsequent figure Φ runs from $\pi/2$ to $5\pi/2$.

The horizontal location x and moving direction Φ are directly coupled in the last term on the right side, which is of the order of dt. We have checked that this third term can be neglected in our model, both in terms of any qualitative predictions but also (and perhaps more surprisingly) at little cost in quantitative accuracy even though our model involves discrete update steps. Consequently, Eq(9) can be simplified to

$$\frac{\partial p}{\partial t} = -\frac{\partial p}{\partial x} v\cos(\Phi) + \frac{\sigma(x)^2}{2}\frac{\partial^2 p}{\partial \Phi^2} \tag{9}$$

Following standard procedures (For example, see ref [31]), one can show the Langevin equations below are equivalent to the Fokker-Planck approach:

$$\begin{aligned} \frac{dx}{dt} &= v\cos(\Phi) \\ \frac{d\Phi}{dt} &= \eta(t) \end{aligned} \tag{10}$$

where $\langle \eta(t) \rangle = 0, \langle \eta(t)\eta(t') \rangle = \delta(t - t')\sigma(x)^2$.

We then solve Eq (9) for both the uniform and stiffness gradient substrate cases. Fig 4a shows the initial condition in the all cases discussed in the following; in particular we apply a narrow gaussian distribution to approximate the δ in $p(x, \Phi; t = 0) = \frac{1}{2\pi}\delta(x), \Phi \in (0, 2\pi)$. The solution shows a peak in x which varies from being at positive values (for $\Phi \simeq 0$) to negative ones (for $\Phi \simeq \pi$); the peak heights are independent of Φ as expected via rotational symmetry (see Fig 4b).

For the stiffness gradient case, the stiffness distribution is described by Eq (5) with $L = 400$. The full distributions are shown at several times in Figs. 5a and 5b. Now there is a clear peak as a function of the direction. Most cells adapt their moving directions from their initial directions $\Phi(t = 0)$ to Φ near zero, exhibiting durotaxis (data not shown); this can be seen by showing a full 2d density plot, where there is a sharp ridge of cells moving ahead and a significant smearing of cells that are going backwards (Fig 5c). This can be studied by defining $\hat{p}(x, t) = \int_0^{2\pi} p(x, \Phi, t) d\Phi$ and comparing our PDE result

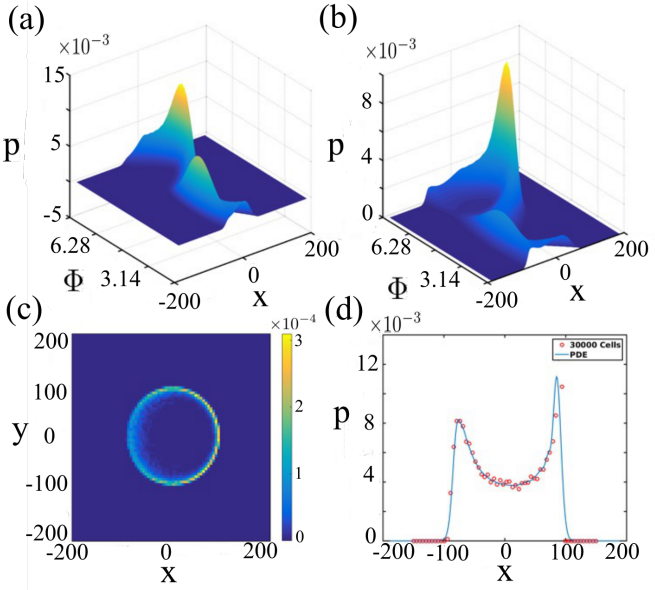

FIG. 5: *PDE solution and comparison to simulation on a substrate with stiffness gradient.* Probability density distribution $p(x, \Phi; t)$ at (a) t=56 (b) t=94. (c) Full 2d density plot, from direct simulation, (d) Comparison between direct simulations of 30000 cells and the numerical solution of the Fokker-Planck equation for $\hat{p}(x, t = 94)$.

for this quantity with direct simulations (Fig 5d). The very good agreement between PDE and direct simulation results validates the Fokker-Planck equation approach. Note that as time progresses the above trends continue, with the population continuing to break up into a peak at positive x and a straggler peak at negative x corresponding to cells that have wandered out into the uniform less stiff side of the gradient profile.

In general, the Fokker-Planck approach is computationally preferable, especially if we are interested in long-time behavior of the density. With direct simulation, we often need to calculate many thousands of cells to determine a smooth distribution. An example is shown in Fig 6a, where the left side of the box is soft, the right half hard and we have used reflective boundary conditions in x and periodic in y. Even though the trajectories are very different on each side, the overall steady-state density distribution is flat (see Fig. 6). This can be obtained directly from the steady-state Fokker-Planck approach, either by numerical relaxation or analytically by separation of variables.

To see one last non-trivial use of the PDE approach, we now generalize our model to allow the velocity to be stiffness dependent. The Fokker-Planck equation now becomes

$$\frac{\partial p}{\partial t} = -\cos(\Phi)\frac{\partial}{\partial x}(pv(x)) + \frac{\sigma(x)^2}{2}\frac{\partial^2 p}{\partial \Phi^2} \tag{11}$$

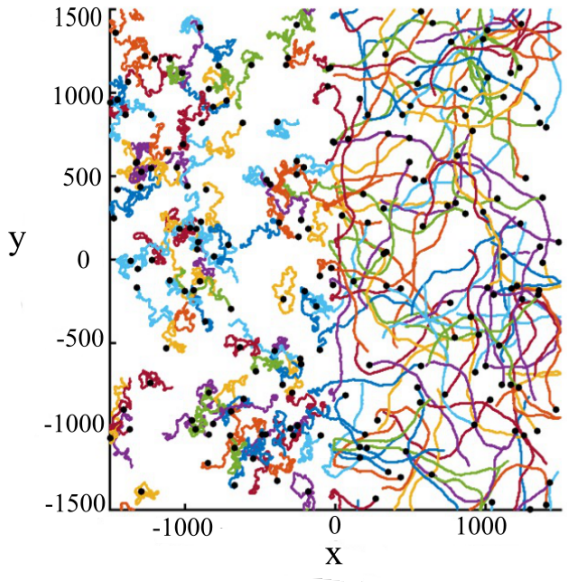

FIG. 6: *Direct simulations with random initial velocities velocity and uniform initial spatial density.*

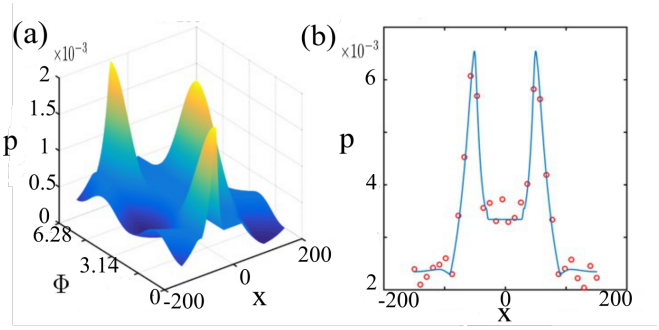

FIG. 7: *Further test of the PDE* (a) Full PDE solution for periodic variation in stiffness and concomitant cell speed, with random initial velocities velocity and uniform initial spatial density. (b) Comparison between direct simulations of 10000 cells and the numerical solution of the Fokker-Planck equation for $\hat{p}(x, t = 200)$

We use the specific forms

$$k(x) = \begin{cases} k_{hard} = 5 & -150 < x < -90 \\ k_{hard} + \frac{(k_{soft} - k_{hard})}{60}(X + 90) & -90 \leq X \leq -30 \\ k_{soft} = 1 & -30 < x < 30 \\ k_{soft} + \frac{(k_{hard} - k_{soft})}{60}(X - 30) & 30 \leq X \leq 90 \\ k_{hard} = 5 & 90 < x < 150 \end{cases} \tag{12}$$

and for the same regions,

$$v(x) = \begin{cases} v_{hard} = 0.56 \\ ((\frac{\sqrt{v(soft)} - \sqrt{v(hard)}}{60} * (x + 90) + \sqrt{v(hard)})^2 \\ v_{soft} = 0.0165 \\ ((\frac{-\sqrt{v(soft)} + \sqrt{v(hard)}}{60} * (x - 30) + \sqrt{v(soft)})^2 \\ v_{hard} = 0.56 \end{cases} \tag{13}$$

Fig 7 shows that the PDE result matches very well with direction simulation, but direction simulation needs a very large amount of cells to get a smooth result.

In this study, we discussed a possible underlying mechanism for durotaxis, namely a stiffness dependence of FA formation and possible FA-dependent speed. It is known that FAs can dynamically sample rigidity to act as mechanosensors [25], but it remains elusive how FAs formation can directly control cell motility. In previous work, it has been shown that stiffness dependent persistence time leads to durotaxis [19]. In our work, we proposed several biophysical mechanisms that can cause positive correlation between persistence time and/or distance and substrate stiffness. For example, we show that a model starting from stiffness dependent FA formation assumption can generate consistent results to those in [19]. In addition, we derived the corresponding 2D Fokker-Planck equation associated with our model and show that it gives consistent numerical agreement with our simulations. To show some novel application of our model, we predicted long-term durotaxis effects on cell density distribution in the presence of a spatially-complex stiffness field. We find that the velocity dependency on stiffness can lead to cell trapping on soft materials. Our work can potentially help in predicting cell motility in more complex physiological environments such as those arising during cancer metastasis.

Our model implicitly assumes that cells are incompetent at sensing rigidity gradients without moving around. For chemotaxis, a close analog of durotaxis, a eukaryotic cell is capable of comparing chemical concentration between its two ends, even though a typical bacterium bacteria is not [32]. It is technically hard to test such an ability in durotaxis, mainly because the cytoskeleton is essential for both cell motility and mechanosensing. Recently it has been shown that some cells can exhibit durotaxis as a cluster even if isolated constituent cells are ineffective [33]; in this case motion appears to not be necessary.

Acknowledgements. This work was supported by the National Science Foundation Center for Theoretical Biological Physics (Grant NSF PHY-1427654). HL was also supported by the CPRIT Scholar program of the State of Texas.

[1] Ning Wang, James P Butler, Donald E Ingber, et al. Mechanotransduction across the cell surface and through the cytoskeleton. *Science*, 260(5111):1124–1127, 1993.

[2] Farshid Guilak, Daniel M Cohen, Bradley T Estes, Jeffrey M Gimble, Wolfgang Liedtke, and Christopher S Chen. Control of stem cell fate by physical interactions with the extracellular matrix. *Cell stem cell*, 5(1):17–26, 2009.

[3] Jennifer S Park, Julia S Chu, Anchi D Tsou, Rokhaya Diop, Zhenyu Tang, Aijun Wang, and Song Li. The effect of matrix stiffness on the differentiation of mesenchymal stem cells in response to tgf-β. *Biomaterials*, 32(16):3921–3930, 2011.

[4] Nicholas D Evans, Caterina Minelli, Eileen Gentleman, Vanessa LaPointe, Sameer N Patankar, Maria Kallivretaki, Xinyong Chen, Clive J Roberts, and Molly M Stevens. Substrate stiffness affects early differentiation events in embryonic stem cells. *Eur Cell Mater*, 18(1):e13, 2009.

[5] Britta Trappmann, Julien E Gautrot, John T Connelly, Daniel GT Strange, Yuan Li, Michelle L Oyen, Martien A Cohen Stuart, Heike Boehm, Bojun Li, Viola Vogel, et al. Extracellular-matrix tethering regulates stem-cell fate. *Nature materials*, 11(7):642–649, 2012.

[6] Robert J Pelham and Yu-li Wang. Cell locomotion and focal adhesions are regulated by substrate flexibility. *Proceedings of the National Academy of Sciences*, 94(25):13661–13665, 1997.

[7] Tony Yeung, Penelope C Georges, Lisa A Flanagan, Beatrice Marg, Miguelina Ortiz, Makoto Funaki, Nastaran Zahir, Wenyu Ming, Valerie Weaver, and Paul A Janmey. Effects of substrate stiffness on cell morphology, cytoskeletal structure, and adhesion. *Cell motility and the cytoskeleton*, 60(1):24–34, 2005.

[8] Chun-Min Lo, Hong-Bei Wang, Micah Dembo, and Yu-li Wang. Cell movement is guided by the rigidity of the substrate. *Biophysical journal*, 79(1):144–152, 2000.

[9] Lars Bollmann, David E Koser, Rajesh Shahapure, Hélène OB Gautier, Gerhard A Holzapfel, Giuliano Scarcelli, Malte C Gather, Elke Ulbricht, and Kristian Franze. Microglia mechanics: immune activation alters traction forces and durotaxis. *Frontiers in cellular neuroscience*, 9, 2015.

[10] Markus Basan, Jens Elgeti, Edouard Hannezo, Wouter-Jan Rappel, and Herbert Levine. Alignment of cellular motility forces with tissue flow as a mechanism for efficient wound healing. *Proceedings of the National Academy of Sciences*, 110(7):2452–2459, 2013.

[11] Vicki P Losick, Donald T Fox, and Allan C Spradling. Polyploidization and cell fusion contribute to wound healing in the adult drosophila epithelium. *Current Biology*, 23(22):2224–2232, 2013.

[12] Sui Huang and Donald E Ingber. Cell tension, matrix mechanics, and cancer development. *Cancer cell*, 8(3):175–176, 2005.

[13] Sudhakar K Venkatesh, Meng Yin, James F Glockner, Naoki Takahashi, Philip A Araoz, Jayant A Talwalkar, and Richard L Ehman. Mr elastography of liver tumors: preliminary results. *American Journal of Roentgenology*, 190(6):1534–1540, 2008.

[14] R Sambeth and A Baumgaertner. Autocatalytic polymerization generates persistent random walk of crawling cells. *Physical review letters*, 86(22):5196, 2001.

[15] S Huang, CP Brangwynne, KK Parker, and DE Ingber. Symmetry-breaking in mammalian cell cohort migration during tissue pattern formation: Role of random-walk persistence. *Cell motility and the cytoskeleton*, 61(4):201–213, 2005.

[16] Zeinab Sadjadi, M Reza Shaebani, Heiko Rieger, and Ludger Santen. Persistent-random-walk approach to anomalous transport of self-propelled particles. *Physical Review E*, 91(6):062715, 2015.

[17] AM Reynolds. Can spontaneous cell movements be modelled as lévy walks? *Physica A: Statistical Mechanics and its Applications*, 389(2):273–277, 2010.

[18] Sergey V Buldyrev, Ary L Goldberger, Shlomo Havlin, Chung-Kang Peng, Michael Simons, and H Eugene Stanley. Generalized lévy-walk model for dna nucleotide sequences. *Physical Review E*, 47(6):4514, 1993.

[19] Elizaveta A Novikova, Matthew Raab, Dennis E Discher, and Cornelis Storm. Persistence-driven durotaxis: Generic, directed motility in rigidity gradients. *Physical Review Letters*, 118(7):078103, 2017.

[20] Oliver T Fackler and Robert Grosse. Cell motility through plasma membrane blebbing. *The Journal of cell biology*, 181(6):879–884, 2008.

[21] Kinneret Keren. Cell motility: the integrating role of the plasma membrane. *European Biophysics Journal*, 40(9):1013–1027, 2011.

[22] Vitold E Galkin, Albina Orlova, and Edward H Egelman. Actin filaments as tension sensors. *Current Biology*, 22(3):R96–R101, 2012.

[23] Pieta K Mattila and Pekka Lappalainen. Filopodia: molecular architecture and cellular functions. *Nature reviews Molecular cell biology*, 9(6):446–454, 2008.

[24] Dong-Hwee Kim and Denis Wirtz. Focal adhesion size uniquely predicts cell migration. *The FASEB Journal*, 27(4):1351–1361, 2013.

[25] Sergey V Plotnikov, Ana M Pasapera, Benedikt Sabass, and Clare M Waterman. Force fluctuations within focal adhesions mediate ecm-rigidity sensing to guide directed cell migration. *Cell*, 151(7):1513–1527, 2012.

[26] Léa Trichet, Jimmy Le Digabel, Rhoda J Hawkins, Sri Ram Krishna Vedula, Mukund Gupta, Claire Ribrault, Pascal Hersen, Raphaël Voituriez, and Benoît Ladoux. Evidence of a large-scale mechanosensing mechanism for cellular adaptation to substrate stiffness. *Proceedings of the National Academy of Sciences*, 109(18):6933–6938, 2012.

[27] Brett C Isenberg, Paul A DiMilla, Matthew Walker, Sooyoung Kim, and Joyce Y Wong. Vascular smooth muscle cell durotaxis depends on substrate stiffness gradient strength. *Biophysical journal*, 97(5):1313–1322, 2009.

[28] Danying Shao, Herbert Levine, and Wouter-Jan Rappel. Coupling actin flow, adhesion, and morphology in a computational cell motility model. *Proceedings of the National Academy of Sciences*, 109(18):6851–6856, 2012.

[29] Matthew Raab, Joe Swift, PC Dave P Dingal, Palak Shah, Jae-Won Shin, and Dennis E Discher. Crawling from soft to stiff matrix polarizes the cytoskeleton and phosphoregulates myosin-ii heavy chain. *The Journal of cell biology*, 199(4):669–683, 2012.

[30] Matthew Raab, Joe Swift, PC Dave P Dingal, Palak Shah, Jae-Won Shin, and Dennis E Discher. Crawling from soft to stiff matrix polarizes the cytoskeleton and phosphoregulates myosin-ii heavy chain. *The Journal of cell biology*, 199(4):669–683, 2012.

[31] Robert Zwanzig. *Nonequilibrium statistical mechanics*. Oxford University Press, 2001.

[32] Guenther Witzany and Mariusz Nowacki. *Biocommunication of ciliates*. Springer, 2016.

[33] Raimon Sunyer, Vito Conte, Jorge Escribano, Alberto Elosegui-Artola, Anna Labernadie, Léo Valon, Daniel Navajas, José Manuel García-Aznar, José J Muñoz, Pere Roca-Cusachs, et al. Collective cell durotaxis emerges from long-range intercellular force transmission. *Science*, 353(6304):1157–1161, 2016.